IEEE Access
Multidisciplinary ⋮ Rapid Review ⋮ Open Access Journal

Received March 11, 2022, accepted March 28, 2022, date of publication April 5, 2022, date of current version April 14, 2022.

Digital Object Identifier 10.1109/ACCESS.2022.3165035

Dynamic Performance Evaluation of Photovoltaic Three-Diode Model-Based Rung-Kutta Optimizer

MOHAMED F. KOTB[1], (Senior Member, IEEE), ATTIA A. EL-FERGANY[2], (Senior Member, IEEE), EID ABDELBAKI GOUDA[1], AND AHMED M. AGWA[3,4]

[1]Electrical Engineering Department, Faculty of Engineering, Mansoura University, Mansoura 35516, Egypt
[2]Department of Electric Power and Machines, Faculty of Engineering, Zagazig University, Zagazig 44519, Egypt
[3]Department of Electrical Engineering, College of Engineering, Northern Border University, Arar 1321, Saudi Arabia
[4]Prince Faisal bin Khalid bin Sultan Research Chair in Renewable Energy Studies and Applications (PFCRE), Northern Border University, Arar 1321, Saudi Arabia

Corresponding author: Mohamed F. Kotb (mohamadfawzi@gmail.com)

This work was supported by the Deputyship for Research and Innovation, Ministry of Education in Saudi Arabia, under Project IF_2020_NBU_411.

ABSTRACT This paper employs the Rung-Kutta optimizer (RKO) to investigate and analyze the dynamic performance of PV units represented using three-diode model (TDM). The paper can be categorized into three phases; In phase one, efforts are exerted to adapt the proposed optimizer RKO for extracting the optimal unknown parameters of the TDM for two widely used PV units namely PWP201/36 and STM6-40/36 modules. In the second phase, comprehensive comparisons between different recent well-known and challenging optimizers such as interior search algorithm, heap-based optimizer, artificial ecosystem-based optimizer, particle swarm optimizer and many more versus the RKO to indicate its effectiveness and viability. It can be confirmed after fair investigations that the RKO generates the lowest value of the root mean square errors (i.e. 2.050683 mA and 1.712171 mA for TDM PWP201/36 and TDM STM6-40/36 modules, respectively) In addition to that, other comparisons between one-, two- and three-diode models (i.e. SDM, DDM and TDM) using the RKO and other optimizers are made. Lastly, the optimal cropped parameters of the PWP201/36 module are used to create a full Simulink model when it is loaded by switched reluctance motor to analyze and study the dynamic performance of this PV module as a representative case under varied loading scenarios. Many parameters in regards to the SRM and behavior of the PV unit are traced and expansively discussed. It can be stated that the investigated results and comparisons indicate apparently the viability of the RKO improving the PV performance and suggests it to tackle other engineering optimization problems.

INDEX TERMS Models of solar generating units, parameters' extraction, optimization methods, dynamic performance assessments, switched reluctance motor.

I. INTRODUCTION

Renewable energy resources (RES) became a vital replacement to the conventional ones which have high side effects to the environment plus high cost and began to shrink. RESs are infinite and inexhaustible. Most of RES investments are spent on materials and workmanship to build and maintain the facilities, rather than on costly energy imports. The photovoltaic (PV) generation systems (PVGS) are considered one of the better RESs with low environmental footprint, return on investment, lower maintenance, secured long-term cost of the energy, sustainable, and viable source [1]–[5]. PVGSs face many challenges as its generation changeability due to environmental conditions, nonlinear behavior, devices depreciation, required wide areas for large plants, and expensive storage arrangements [6], [7]. A lot of research papers have been introduced to overcome these problems and obtain the best PV performance. To achieve this goal, a reliable modelling and simulation of PV units in addition to precise estimation of its unknown parameters became mandatory [5], [6]. The values of PV parameters substantially affect the efficacy of the system. The PV estimation faces

The associate editor coordinating the review of this manuscript and approving it for publication was Easter Selvan Suviseshamuthu.

many challenges as large computations operations, having local goals, and difficulties with defining the fine settings of the algorithms and its limitations [5], [8]. The best PV operation mainly depends on its parameters determination precision which may change because of varied weather status and cells aging. PV should be represented and simulated as nonlinear problem with numerous variables to achieve these optimal parameters. PV has been modelled as current source with single-, double-, or three-diode model (SDM), (DDM), and (TDM), respectively which require identifying five, seven, and nine unknown parameters in sequence [5]–[10]. Although SDM and DDM have quick response, both neglect leakage, diffusion, and recombination losses which have been considered by TDM [10]. Many efforts have been done to get the best PV performance using analytical, deterministic, and metaheuristic approaches [11]–[17]. Although analytical methods are simple and fast to obtain the results, they have large calculation steps and lack of accurateness [13]–[17]. Deterministic tactics have more accuracy but faces problems with identifying the preliminary starting points that may cause divergence leading to go to topical goals away from the main objective because of its iterative nature or using trial and error technique [14]–[19]. Metaheuristic methods have been introduced to overcome the mentioned drawbacks by matching between investigation and the manipulation stages. Metaheuristic methods have been applied to several power system areas as particle swarm optimization (PSO) for optimal power flow [20], whale optimization algorithm (WOA) for resource allocation [21], hybrid multi-objective approach for economic load dispatch [22], and evolutionary grey wolf optimizer for scheduling problem [23]. In this concern, many outstanding efforts have been exerted in extracting PV unknown parameters for the three models namely SDM, DDM, and TDM. For example, WOA based reflecting learning [24] and improved electromagnetism-like algorithm using nonlinear equations [25] have been utilized for extracting unknown parameters of SDM. Much researches have been presented for both SDM and DDM as following. Classified perturbation mutation based PSO algorithm proofed steady and efficient algorithm but with long execution time [13]. Enhanced adaptive differential evolution algorithm which could facilitate transferring of the best searching elements to the following step and shorten execution time by employing energetic population [14]. Performance-guided Jaya which could improve searching elements by self-controlling of the disordered elements [26]. Salp swarm algorithm which consider parameters uncertainty [27]. Improved teaching-learning-based optimization could develop a new learning method for the populations to reach the solution faster [28]. Grey wolf optimizer and cuckoo search used novel antagonism [29]. Biogeography-based heterogeneous cuckoo search who integrated the advantages of cuckoo and biogeography procedures [30]. Additionally, other optimization algorithms have been utilized for parameters identifications of SDM and/or DDM of PVGS such as Levenberg-Marquardt algorithm [31], backtracking seeking approach [32], approximating and correcting procedure [33], highest likelihood estimator [34], imperialist competitive approach [35], interior seeking optimizer [36], counteraction-based sine cosine algorithm [37], and support vector machine [38]. Few researches have been introduced for modelling TDM. Harris hawk's optimization extracted only five parameters and calculated the other four parameters using derivative equations [26]. Grasshopper optimization algorithm [39] and artificial electric field algorithm (AEFA) [40] could extract the nine parameters for commercial PV modules and study the PV units under different operating conditions. Manta-rays foraging optimizer have been utilized using three main points known by manufacturer information and two groups taken by measurements for I/V characteristics of PVGSs [41].

The major goal of this work is to effectively represent the PV units thru optimal identification of its uncertain parameters and study its steady-state and dynamic performances. Runge-Kutta optimizer (RKO) is an original metaheuristic optimizer utilized to erratically and preciously identify the PV parameters represented as TDM based on Runge-Kutta (RK) method [42]. It is considered a robust and fast technique using groups of motivated rules for exploration. RKO has been used to solve the sensitive wave propagation problems [43]. The RKO depends mainly on maximizing its order to assure the solution accurateness and minimizing the number of phases to reduce the amount of the required calculations. It has an efficient capability for best utilization of dynamic investigation and manipulation phases in the promising space going to the comprehensive best goal while avoiding the obsesses of metaphors. Fifty scientific functions and four practical engineering problems that were applied by previous metaheuristic methods have been reevaluated by the RKO [42]. The last proves talented and modest solutions in addition to fast execution and its ability to exclude the local optima for extracting the unknown parameters as in PV.

The proposed RKO is applied to the well-known commercial PWP201/36 and STM6-40/36 PV to analyze and study its performance. Comprehensive comparison between the TDM, DDM, and SDM models using RKO and other reported competitors. For extra authentications, PWP201/36 module is simulated using MATLAB/Simulink and connected to switched reluctance motor (SRM) to assess and analyses its dynamic performance.

The text of this paper encloses seven sections: Section I announces the Introduction, In Section II, mathematical modelling for different PV units is introduced. The optimization problem is formulated and adapted which is presented in Section II. In Section IV, the RKO is explained and its procedures are instructed. The application and validation of the studied PV units are examined to extract its unknown parameters in Section V. While the dynamic performance of the PWP201/36 module is studied when it is connected to SRM in Section VI. Finally, the concluding findings and the paper footprint are emphasized in Section VII.

II. MATHENATICAL MODELS OF PVGS USING TDM AND STATEMENT

In an ideal condition, the solar cell is electrically equivalent to a current source in parallel with a number of diodes (D) based on the model used. The light-generated photo current (I_{photo}) increases linearly with sun irradiance. The current travels through semiconductor material which has certain resistivity that can be represented as R_{sr}. As the PVGSs are fabricated of large area wafers, several shunt resistive losses occur at n-layer of the p–n junction of the cell. This is generally represented by a lumped shunt resistor (R_{sh}). Three-diodes (D1 to D3) are used to simulate the influence of grain boundaries and leakage current through the peripheries to form TDM. The complete TDM is illustrated in Fig. 1 and the branches current can be represented in (1) to (6).

$$I_{Solar} = I_{photo} - I_{D1} - I_{D2} - I_{D3} - I_{sh} \tag{1}$$

$$I_{D1} = I_{sat1}\left[exp\left(\frac{VS_{solar}+I_{Solar}.R_{sr}}{\beta_1.V_{TM}}\right) - 1\right] \tag{2}$$

$$I_{D2} = I_{sat2}\left[exp\left(\frac{VS_{solar}+I_{Solar}.R_{sr}}{\beta_2.V_{TM}}\right) - 1\right] \tag{3}$$

$$I_{D3} = I_{sat3}\left[exp\left(\frac{VS_{solar}+I_{Solar}.R_{sr}}{\beta_3.V_{TM}}\right) - 1\right] \tag{4}$$

$$V_{TM} = \frac{K_{Bot}.T_{emp}}{Q_e} \tag{5}$$

$$I_{sh} = \frac{VS_{solar} + I_{Solar}.R_{sr}}{R_{sh}} \tag{6}$$

where $I_{Solar}, I_{D1}, I_{D2}, I_{D3}, I_{sat1}, I_{sat2}, and\ I_{sat3}$ are the PV output current, diodes currents D1, D2, and D3, and their saturation currents, respectively. The output cell voltage, the thermal voltage, the cell temperature, Boltzmann constant, electron charge, quality factors of diodes, series, and shunt resistance are represented as VS_{solar}, V_{TM}, T_{emp}, K_{Bot}, Q_e, β_1, β_2, β_3, R_{sr}, and R_{sh}, correspondingly.

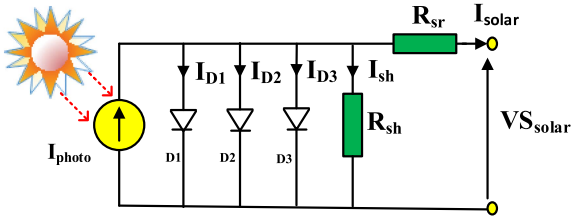

FIGURE 1. Equivalent circuit of the TDM.

N_s is the number of PV cells and organized in series to form module voltage, in which $VS_{Module} = N_s \times VS_{solar}$ and module current (I_{Module}) is equal to I_{Solar}.

The PV parameters at rated standard conditions (RSC) and any other running conditions are given by the following (7) to (12) [10].

$$I_{photo} = I_{photo-N}\frac{G}{G_N}\left[1 + \propto_I (T - T_N)\right] \tag{7}$$

$$R_{sh} = \frac{G_N}{G}R_{sh-N} \tag{8}$$

$$E_g = E_{gN}\left[1 - 2.6677.10^{-4}(T - T_N)\right] \tag{9}$$

$$I_{sat1} = I_{sat1-N}\left(\frac{T}{T_N}\right)^3 exp^{\frac{Q_e E_g}{\beta_1 K_{Bot}}\left(\frac{1}{T_N}-\frac{1}{T}\right)} \tag{10}$$

$$I_{sat2} = I_{sat2-N}\left(\frac{T}{T_N}\right)^3 exp^{\frac{Q_e E_g}{\beta_2 K_{Bot}}\left(\frac{1}{T_N}-\frac{1}{T}\right)} \tag{11}$$

$$I_{sat3} = I_{sat3-N}\left(\frac{T}{T_N}\right)^3 exp^{\frac{Q_e E_g}{\beta_3 K_{Bot}}\left(\frac{1}{T_N}-\frac{1}{T}\right)} \tag{12}$$

where $I_{photo-N}$, G_N, T_N, R_{sh-N}, E_{g-N}, I_{sat1-N}, I_{sat2-N}, I_{sat3-N}, G, E_g, and $\propto_I$ are rated light generated current, rated irradiance, rated temperature, rated shunt resistance, rated energy-band gap, rated first, second and third diode saturation currents, actual irradiance, operation energy band gap, and temperature coefficient of current, respectively. According to the previous TDM's equations, nine parameters i.e. (I_{photo}, I_{sat1}, I_{sat2}, I_{sat3}, β_1, β_2, β_3, R_{sr}, and R_{sh}) should be defined optimally using the RKO in this current effort.

III. OPTIMIZATION OF PV PARAMETERS IDENTIFICATION

The key goal of the PV cells modeling is to find the proper equivalent circuit to simulate it precisely for imitating the practical operations. This should be done at a minimum error level between the experimental and the calculated dataset points. The objective function (F_{obj}) is defined as minimizing the root-mean squared error (RMSE) of the current errors between estimated and measured dataset points which is expressed in (13) as follows:

$$F_{obj} = \text{minimize}\left(\sqrt{\frac{1}{m}\sum_{i=1}^{m}(I_{solar-i}^{meas} - I_{solar-i}^{calc})^2}\right) \tag{13}$$

where, m is the number of measured points, $I_{solar-i}^{meas}$ is the measured current and $I_{solar-i}^{calc}$ is the calculated current. The problem min/max constraints are characterized in (14) for the nine parameters to be extracted.

$$\left\{\begin{array}{l} I_{photo-min} \le I_{photo}(A) \le I_{photo-max} \\ I_{sat-min} \le I_{sat1}, I_{sat2}, I_{sat3}(\mu A) \le I_{sat-max} \\ R_{sr-min} \le R_{sr}(\Omega) \le R_{sr-max} \\ R_{sh-min} \le R_{sh}(\Omega) \le R_{sr-max} \\ \beta_{min} \le \beta_1, \beta_2, \beta_3 \le \beta_{max} \end{array}\right\} \tag{14}$$

where, $I_{photo-min}$ and $I_{photo-max}$ are the min/max values of I_{photo}, $I_{sat-min}$ and $I_{sat-max}$ are the min/max of I_{sat}, R_{sr-min} and R_{sr-max} are the min/max limits of R_{sr}, R_{sh-min} and R_{sh-max} are the min/max of R_{sh} and β_{min} and β_{min} are the min/max limits of β_1, β_2 and β_3.

IV. RKO OPTIMIZER PROCEDURE

The RKO is a new swarm-based version with elements randomly determined based on RK method. RKO utilizes the suggested slope of the fourth derivative of RK method (RK4) to logically look for the best area in the searching space for generating a group of rules. RK technique (RKT) has

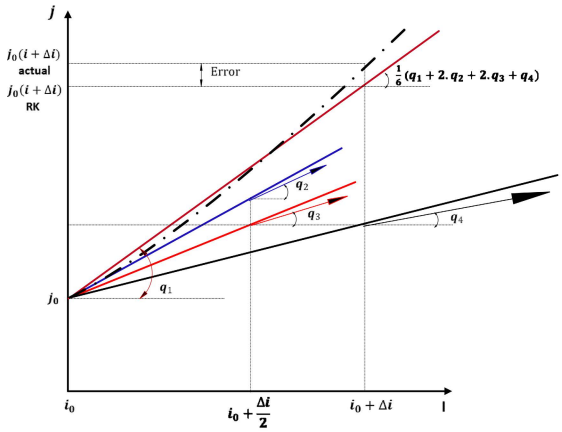

(a) RK Initial Location and slopes

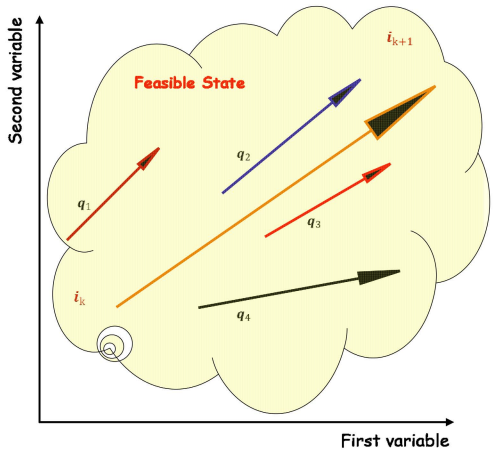

(b) Updating the location (i_{k+1}) in the RKO algorithm

FIGURE 2. RK method.

high accurateness in solving the regular differential equations without need for high-order derivatives. It avoids the local optima and is characterized by some groups of motivated rules at appropriate time instead of metaphor tongue [42].

The main concept of RKT is to identify the slope S = f(i, j) of the finest straight line tailored to the graph at the point (i, j). The first-order common differential equation can be expressed in (15) for an initial value problem.

$$\frac{\mathrm{dj}}{\mathrm{di}} = \mathrm{f(i,j)} = \mathrm{S}, \quad \mathrm{j(i_0)} = \mathrm{j_0} \tag{15}$$

Starting by initial point (i_0, j_0) with an original slope, there is another point (i_1, j_1) can be extracted utilizing the most excellent customized straight line as $(i_1, j_1) = (i_0 + \Delta I, j_0 + S_0.\Delta i)$ where the initial slop is $S_0 = f(i_0, j_0)$. The same can be applied for another point, $(i_2, j_2) = (i_1 + \Delta i, j_1 + S_1.\Delta i)$ where the new slop is $S_1 = f(i_1, j_1)$. This process can be repeated "n" times to get approximate solution in the range of $(i_0, i_0 + n\Delta i)$. The RKT can be formulated as per Taylor series using (16).

$$\mathrm{j(i+\Delta i) = j(i) + j'(i)\Delta i + j''(i)\frac{\Delta i^2}{2!} + \cdots .} \tag{16}$$

The first-order derivative RK1 "$j'(i)''$ is approximated as following:

$$\mathrm{j'(i) = \frac{j(i+\Delta i) - j(i-\Delta i)}{2\Delta i}} \tag{17}$$

The fourth order RK4 can be derived from (16) and represented as shown in Fig. 2 as following:

$$\mathrm{j(i+\Delta i) = j(i) + \frac{1}{6}(q_1 + 2.q_2 + 2.q_3 + q_4)\Delta i} \tag{18}$$

The weighted elements of the first, second, third, and fourth increment are represented by $q_1, q_2, q_3,$ and q_4, respectively and they define the slopes at each interval that can be calculated via (19) as following:

$$\begin{cases} \mathrm{q_1 = j'(i) = f(i,j)} \\ \mathrm{q_2 = j''(i) = f\left(i + \frac{\Delta i}{2}, j + \frac{\Delta i}{2}.q_1\right)} \\ \mathrm{q_3 = i'''(i) = f\left(i + \frac{\Delta i}{2}, j + \frac{\Delta i}{2}.q_2\right)} \\ \mathrm{q_4 = j''''(i) = f\left(i + \frac{\Delta i}{2}, y + \frac{\Delta i}{2}.q_3\right)} \end{cases} \tag{19}$$

The initial locations $i_{k,m}$ for the k^{th} population ($k \in K_{pop}$) of the m^{th} variable ($m \in M$) considering the minimum (Min_m) and maximum (Max_m) boundaries are haphazardly proposed through (20).

$$\mathrm{i_{k,m} = Min_m + Rand1.(Max_m - Min_m)} \tag{20}$$

The introduced optimization applies and utilizes the location i_k instead of the fitness ($j(i_k)$) to save the time consumed in running the F_{obj} of locations. The function j(i) is treated as minimization problem taking the two terms $(i_k + \Delta i)$ and $(i_k - \Delta i)$, two adjacent locations for i_k appeared in (17), as the finest location (i_f) and poorest location (i_p) respectively at each iteration. Then,

$$\mathrm{q_1 = \frac{i_p - i_f}{2\Delta i}} \tag{21}$$

i_f and i_p are defined by selecting three random solutions from the participants of the population (i_{r1}, i_{r2}, i_{r3}) where $r1 \neq r2 \neq r3 \neq k$. To improve the exploration search and to activate the performance of randomness, (21) can be reformulated via (22) and (23).

$$\mathrm{q_1 = \frac{Rand1.i_p - R_O.i_f}{2\Delta i}} \tag{22}$$

$$\mathrm{R_o = Round(1 + Rand1)(1 - Rand1)} \tag{23}$$

where Rand1 is a random value between 0 and 1, R_o is another random value utilized to raise the significance of the where i_f is the finest solution and Δi is the location increment which can be determined as per (24).

$$\left.\begin{aligned} &\Delta i = 2.\text{rand1}.|St| \\ &St = \text{rand1}.[(i_f - \text{Rand1}.i_{av}) + Sf] \\ &Sf = \text{rand1}.(i_k - \text{Rand1}.(R_o - m).\exp(-\frac{4.h}{h_{max}}) \end{aligned}\right\} \quad (24)$$

St is the stage range, depends mainly on the difference between i_f and the average of all solutions i_{av} for one iteration in addition to the scaling factor Sf which exponentially falling with the solution range of the search space during the optimization progression, h is the number of iterations, and h_{max} is the maximum number of iterations. Random values in (24) are used to expedite the divergence and to have wider search space.

Subsequent to the same idea, the other three weighted elements $q_2, q_3,$ and q_4 can be determined as in (25), as shown at the bottom of the page, where $Rand2$ and $Rand3$ are two random numbers in the range of [0, 1] and i_f *and* i_p can be calculated by (26):

$$\left\{\begin{array}{l} If\ f\ (i_k) < f\ (i_{fn}) \\ i_f = i_k \\ i_p = i_{fn} \\ Else \\ i_f = i_{fn} \\ i_p = i_k \end{array}\right\} \quad (26)$$

Therefore, the main exploration technique ET to get the RK location i_{RK} in RKO can be defined as in (27).

$$\left\{\begin{array}{l} ET = \dfrac{1}{6}\ (i_{RK})\ \Delta i \\ i_{RK} = q_1 + 2q_2 + 2q_3 + q_4 \end{array}\right\} \quad (27)$$

The solution can be updated for the following iteration as following in (28):

$$\begin{aligned} &If\ Rand1 < 0.5 \\ &\quad i_{k+1} = i_c + AF.ET + \lambda.i_s \text{“Exploration phase”} \\ &\quad Else \\ &\quad i_{k+1} = i_m + AF.ET + \lambda.i_{s1} \text{“Exploitation phase”} \\ &\quad End \\ &where: \lambda = 0.5 + 0.1Rand4, \\ &\quad i_s = Rand4.\ (i_m - i_c)\ , \end{aligned}$$

TABLE 1. Used PV models datasheet.

Parameter	PWP201	STM6-40/36
Number of series cells/module: N_s	36	36
Number of parallel arrays: N_p	1	1
Number of modules/array: N_a	1	1
The band-gap energy:E_g	1.2	1.2
Open-circuit voltage at test temperature: $V_{oc@T_r}$	16.7785	21.02
Cell Short-circuit current at test temperature: $I_{sc@T_r}$	1.0317	1.663
Test temperature: T_r	45◦C	51◦C
temperature coefficient of the maximum power(1/oc): K_t	-0.43e-2	-0.488e-2
Cell Short-circuit current /Temperature coefficient: K_i	0.80e-3	0.65e-3
Cell temperature coefficient of OC voltage: K_v	-72.5e-3	-3.46e-3

$$\begin{aligned} i_{s1} &= Rand4.\ (i_{r1} - i_{r2}) \\ i_c &= \beta.i_k + (1-\beta)\ .i_{r1} \\ i_m &= \beta.i_f + (1-\beta)\ .i_{mf} \\ AF &= 2\ (0.5 - Rand1)\ .B \\ B &= b1.\exp\left\{-b2.Rand1.\left(\frac{h}{h_{max}}\right)\right\} \end{aligned} \quad (28)$$

where $b1$ and $b2$ are two key constants influence the search. A reasonable balance between exploration and exploitation search can be adapted by AF. The exploration can be improved by increasing AF at early search stages and decreased at later stages to stimulate the exploitation. To investigate the talented locations near to i_c and i_m, (28) can be reformulated as shown in (29).

$$\begin{aligned} &If\ Rand1 < 0.5 \\ &\quad i_{k+1} = i_c + r.AF.g.i_c + AF.ET + \lambda.i_s \text{ Exploration} \\ &\quad Else \\ &\quad i_{k+1} = i_m + r.AF.g.i_m + AF.ET + \lambda.E \text{ xploitation} \\ &\quad End \end{aligned} \quad (29)$$

where r is an element which increases search variety and affects the exploration path with value of 1 or -1 and g is a number haphazardly selected between 0 and 2. The local exploration nearby i_c declines with the increasing the number of iterations.

It can be highlighted here that the RKO is improved for more quality and to evade local targets each iteration to transfer to the finest solution by estimating the average of

$$\left\{\begin{array}{l} q_2 = \dfrac{(Rand1(i_p + Rand2.q_1.\Delta i) - (R_o.i_f + Rand3.q_1.\Delta i}{2\Delta i} \\ q_3 = \dfrac{(Rand1(i_pRand2.[0.5q_2].\Delta i) - (R_o.i_f + Rand3.[0.5q_2]}{2\Delta i} \\ q_4 = \dfrac{(Rand1(i_p + Rand2.q_3.\Delta i) - (R_o.i_f + Rand3.q_3.\Delta i}{2\Delta i} \end{array}\right\} \quad (25)$$

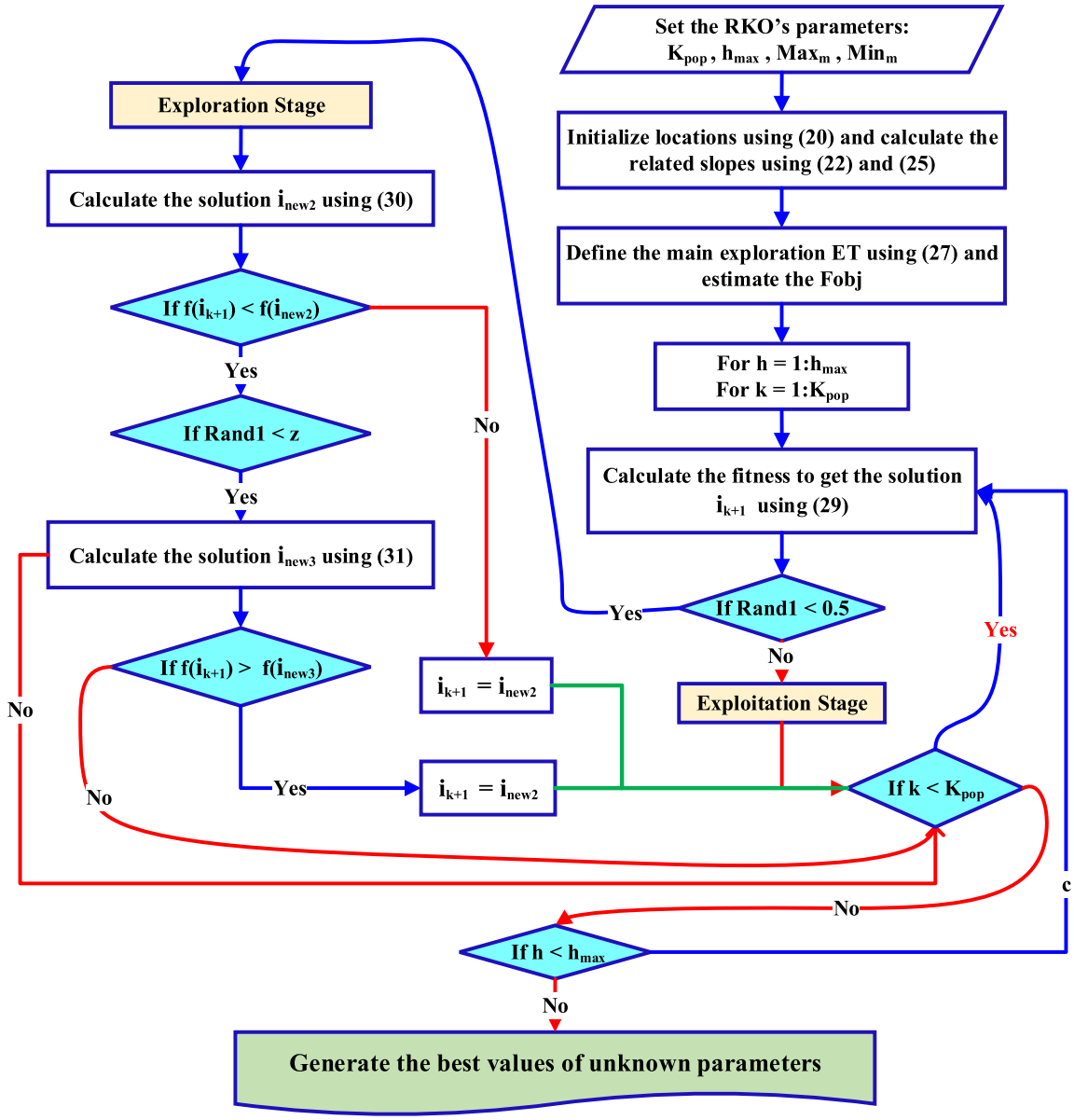

FIGURE 3. RKO optimizer flow chart.

three random solutions i_{av} and to be integrated with the i_f to get a new solution i_{new1} as defined in (30).

$$\left\{\begin{array}{l} If\ Rand1 < 0.5 \\ If\ z < 1 \\ i_{new2} = i_{new1} + r.z.\,|(i_{new1} - i_{new2}) + Rand5| \\ Else \\ i_{new2} = \\ (i_{new1} - i_{av}) + r.z.\,|(R_o.i_{new1} - i_{av}) + Rand5| \\ End \\ End \\ Where: z = Rand\,(0,2)\,.exp\left(-z1\left\{\dfrac{h}{h_{max}}\right\}\right) \\ i_{av} = \dfrac{i_{r1} + i_{r2} + i_{r3}}{3} \\ i_{new1} = \mu.i_{av} + (1-\mu)\,.i_f \end{array}\right. \tag{30}$$

where μ, z1, r and z are random numbers. The value of μ is between 0 and 1, r equals 1,0 or -1, and z1 is 5 times Rand1 and z diminishes by increasing the number of iterations. The solution i_{new2} leads to generate the exploration search when $z \geq 1$ at initial iterations and can produce the exploitation search for $z < 1$ at late iterations. If $f\,(i_{new2}) > f\,(i_k)$, alternative solution i_{new3} can be elaborated by (31) when $Rand\,1 < z$.

$$i_{new3} = (i_{new2} - Rand1.i_{new2}) + AF.(Rand1.i_{LM} + (\delta.i_f - i_{new2})) \tag{31}$$

where δ is a random value equals double Rand. i_{LM} is calculated when i_f and i_z becomes i_k and i_{new2} respectively. The RKO Optimizer process can be summarized as shown in the flow chart in Fig. 3.

TABLE 2. Comparison between proposed RKO and another optimizer for TDM PWP201/36 module (results per cell.).

Parameters	I_{photo} (A)	I_{sat1} (μA)	I_{sat2} (μA)	I_{sat3} (μA)	R_{sr} (Ω)	R_{sh} (Ω)	β_1	β_2	β_3	*RMSE*.e-4
RKO	1.0317	0.00102	0.001	0.00259	0.034400	22.2000	1.390	1.99245	1.3205	20.50683
AEFA [40]	1.0323	1.2616	0.008	0.86557	0.034981	19.9178	1.389	1.38900	1.38900	20.722
PSO [49]	1.0313	10.000	56.137	10.000	1.267452	29.2166	1.2000	1.2000	2.0000	24.435
ISA [49]	1.0317	3.1028	151.02	2665.8	1.215324	23.801	1.3391	1.6664	1.5673	20.956
AEO [49]	1.0285	2.7884	5.8648	2.9211	1.11924	58.5228	1.4197	2.0000	1.4000	31.168
EO [49]	1.0305	148.060	17.965	4.0954	1.207152	29.148	1.6457	1.2033	1.4000	22.570
HBO [49]	1.0282	1.728	88.243	7.2736	1.218096	36.3415	1.2977	1.4322	1.9349	26.453

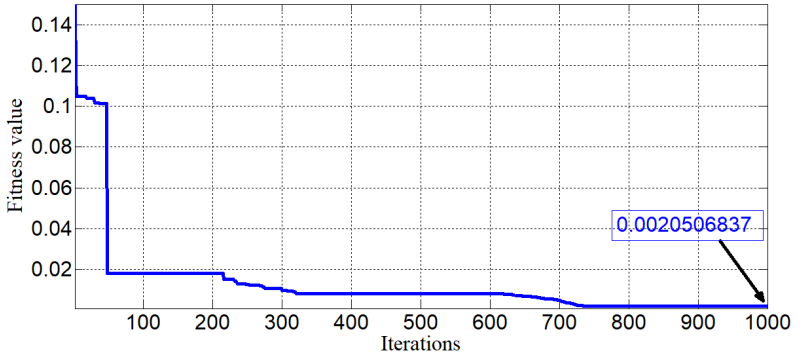

(a) Convergence curve of RKO for TDM PWP201 solar cell

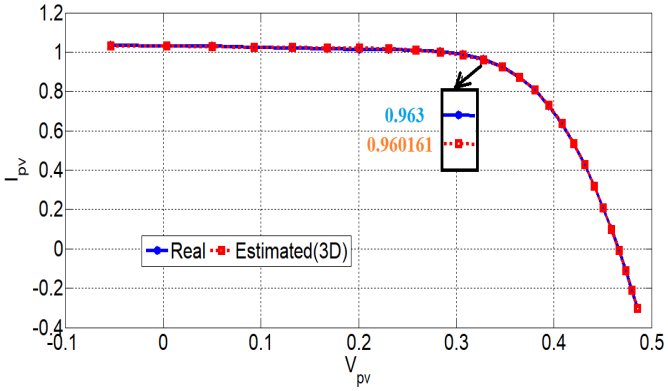

(b) I-V plots

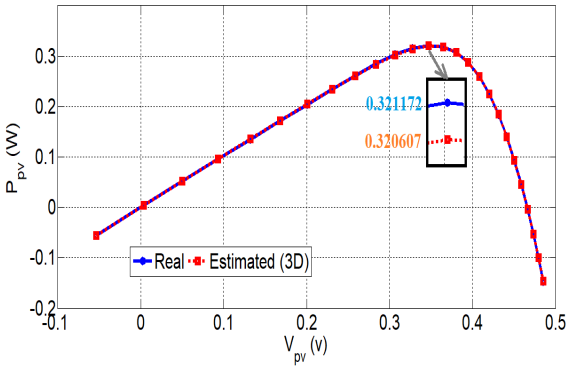

(c) P-V plots

FIGURE 4. Principal performance of RKO for TDM PWP201 solar cell.

TABLE 3. Comparison between proposed RKO and another optimizer for TDM STM6-40/36 module (results per cell.).

Parameters	I_{photo} (A)	I_{sat1} (μA)	I_{sat2} (μA)	I_{sat3} (μA)	R_{sr} (Ω)	R_{sh} (Ω)	β_1	β_2	β_3	*RMSE*.e-4
RKO	1.663	0.943	5.82	0.0325	0.005645	17.8344	1.5276	1.979	1.2520	**17.1217**
AEFA [40]	1.6640	0.636	0.118	1.000	0.004372	15.8375	1.6667	1.5608	1.6667	17.2030
MPA [50]	1.66412	1.24	5.56	2.200	0.13682	15.419	1.4852	2.265	4.7889	17.7800
AVOT [67]	1.6608	0.0170084	6.0148	2.4847	0.00000107444	27.0763	1.99996	1.8769	1.5945	35.3980
TLSBT [67]	1.6647	0	0	2.0232	0.003393953	14.5458	1.5882	2.000	1.5373	22.8640
TST [67]	1.6607	0.0374315	1.2977	3.1457	0.005606477	20.2183	1.39169	1.9389	3.1457	22.0100

V. APPLICATIONS AND VALIDATIONS VIA DEMONSTRATIONS

The RKO is used to extract the three diode PV models parameters using Intel(R) Core (TM) i7-4710HQ CPU@ 2.5GHZ, and 8 GB RAM PC. A 600 population members, 1000 iterations and 5 independent trials are decided for assuring obtaining high accuracy results of the RKO. The IV measured curves for the presented models are used as

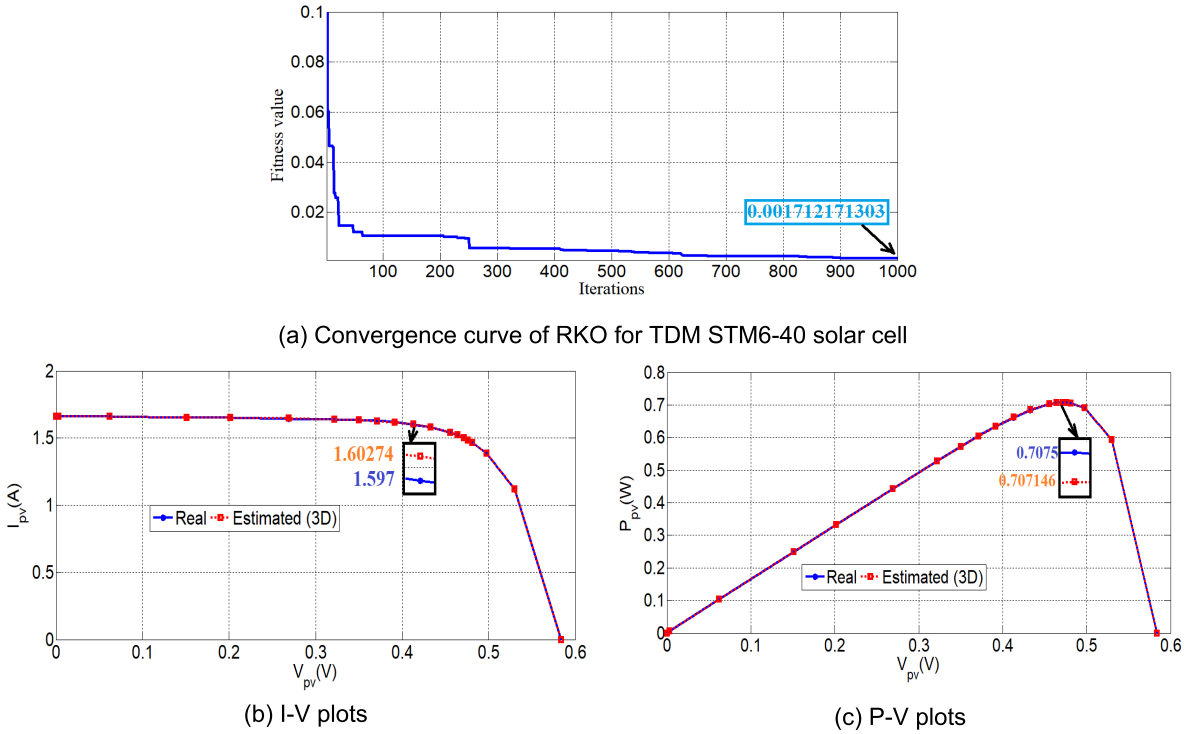

FIGURE 5. Principal performance of RKO for TDM STM6-40 solar cell.

TABLE 4. Comparison between SDM, DDM and TDM using proposed RKO and others for PWP201/36 module.

SDM	Method	RKO	GCPSO [51]	TVACPSO [52]	ICA [52]	ISCE [53]	IWOA [54]	NMSOLMFO [55]	EHA-NMS [56]	TSLLS [57]	RF [58]
	RMSE.e-4	20.400	20.4654	20.530	22.279	24.251	24.251	24.251	24.251	20.465	21.176
DDM	Method	RKO	GCPSO [51]	TVACPSO [52]	CA [52]	TLBO [52]	GWO [52]	FFO [59]	PPSO [60]	GCPSO [51]	
	RMSE.e-4	20.416	20.465	20.530	22.178	22.785	22.138	20.367	21.943	20.465	
TDM	Method	RKO	AEFA [40]	PSO [49]	ISA [49]	AEO [49]	EO [49]	EO [49]	HBO [49]		
	RMSE.e-4	20.501	20.720	24.435	20.956	20.956	31.168	22.570	26.453		

given in [44]–[47]. The two PVGSs namely, PWP201 and STM6-40/36 PV, are studied and analyzed in the subsequent Sections. RKO is utilized to extract uncertain parameters for PWP201 module using SDM and DDM and compared with the TDM using RKO and other trusted and published optimizers. Another comparison between the extracted parameters using various optimizers as SDM, DDM and TDM modelling are made including RKO for TDM for STM6-40/36 PV model. The required basic input information parameters with the corresponding ranges given in Table 1 (data per cell) and in (32) [40], [48].

$$\left\{\begin{array}{l} 0 < \mathrm{I_{photo}}\,(A) < 2 \\ 0 < \mathrm{I_{sat1}}, \mathrm{I_{sat2}}, \mathrm{I_{sat3}}\,(\mu A) < 1 \\ 0 < R_{sr}\,(\Omega) < 0.5 \\ 0 < R_{sh}\,(\Omega) < 100 \\ 1 < \beta_1, \beta_2, \beta_3 < 2 \end{array}\right\} \quad (32)$$

A. APPLICATION OF RKO FOR TDM

The RKO is applied to PWP201 and STM6-40/36 PVGSs to extracted uncertain parameters of TDM of these two units and comparisons to other well-matured optimizers are in order.

1) CASE STUDY OF THE TDM PWP201 UNIT

RKO is applied to TDM PWP201 PVGS and its convergence, I/V and P/V curves are revealed in Fig. 4. The measured and calculated of I/V and P/V characteristics indicated in Figs. 4(b)-(c); respectively show slight error close to MPPT with values 0.295% and 0.175%, correspondingly. The related calculated parameters are tabulated in Table 2 (per cell) and compared with established and published six optimizers (i.e. AFEA [40], PSO [49], interior search algorithm (ISA) [49], artificial eco-system based optimizer (AEO) [49], equilibrium optimizer (EO) [49] and heap-based optimizer (HBO) [49]) for TDM for PWP201/36 unit.

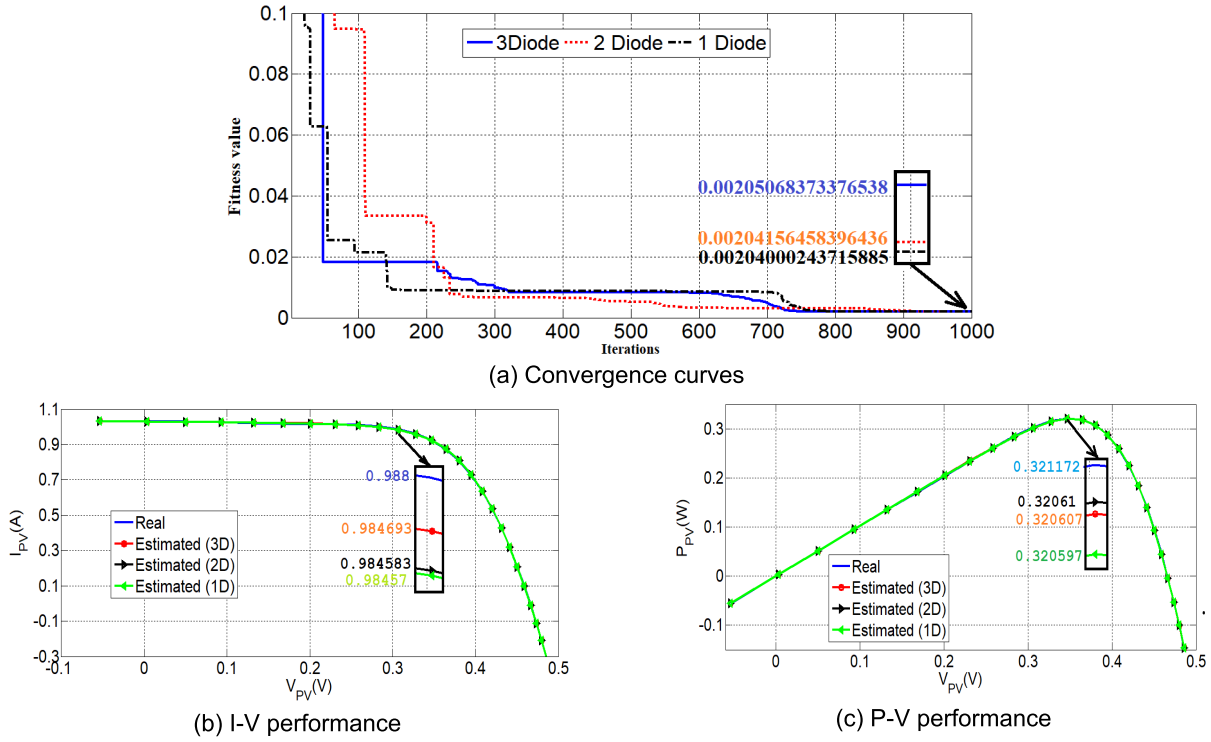

FIGURE 6. Comparison between the TDM, DDM and SDM models for PWP201/36 solar cell when using RKO.

TABLE 5. Comparison between SDM, DDM and TDM using proposed RKO and others for STM6-40/36 module.

SDM	Method	ICSE [53]	SDA [45]	HISA [36]	EHA–NMS [56]	TSLLS [57]	RF [58]	IADE [61]	ICSA [62]	CIABC [64]	CWOA [68]
	RMSE.e-4	17.298	17.2945	17.21921	17.2982	17.6875	30.76954	17.2982	17.9436	18.19	18.0
DDM	Method	ELPSO [65]	CPSO [65]	BSA [65]	ABC [65]	SDO [66]	TLABC [66]				
	RMSE.e-4	18.307	18.343	40.335	20.538	17.298	17.348				
TDM	Method	RKO	AEFA [40]	MPA [50]	AVOT [67]	TLSBT [67]	TST[67]				
	RMSE.e-4	17.122	17.203	17.78	35.398	22.864	22.01				

The RKO achieves significant RMSE improvement by obtaining a lower error of a magnitude of 0.205068373376538 mA after 10000 iterations within 372.5 s.

2) CASE STUDY OF THE TDM STM6-40/36 MODULE

The convergence curves after applying RKO to the TDM STM6-40/36 module are indicated in Fig. 5(a). Comparison between measured and estimated I/V and P/V characteristics shows 0.36% and 0.05% error at nearly MPPT as represented in Fig. 5(b)-(c); respectively. Table 3 indicates the TDM estimated parameters compared to another well-known and trusted optimizer (data per cell) such as AEFA [40], marine predators algorithm (MPA) [50], African vultures optimization technique (AVOT) [67], teaching learning studying-based technique (TLSBT) [67] and Tuna swarm technique (TST) [67]. The RKO proved its effectiveness by resulting a lower value of RMSE of 1.71217130317765 mA takes after 1000 iterations within 39.4 s.

TABLE 6. Motor data.

Stator resistance (Ohm)	Inertia (kg.m.m)	Friction (N.m.s)	Unaligned inductance (H)	Aligned inductance (H)	Saturated inductance (H)
0.05	0.05	0.02	0.67e-3	23.6e-3	0.15e-3

B. COMPARISONS AMONG SDM, DDM AND TDM

The RKO is applied to PWP201 solar cell as TDM, DDM and DDM models. The convergence curves of the three models are shown in Fig. 6(a). It can be noticed that the fitness value has minor difference between the three models, but SDM has the lowest fitness value and TDM has the highest one after the convergence stabilization at 1000 iterations. I/V and P/V performance curves for measured and estimated characteristics are shown in Fig. 5(b)-(c), respectively. A closer look to Table 4, a slight difference in PWP201/36 drawn current is observed between the three models. The PV unit

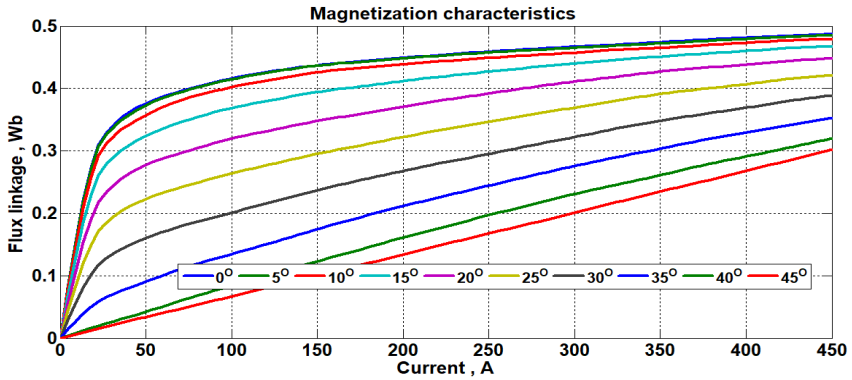

FIGURE 7. The SRM magnetization characteristics (flux linkage versus current at different rotor positions.).

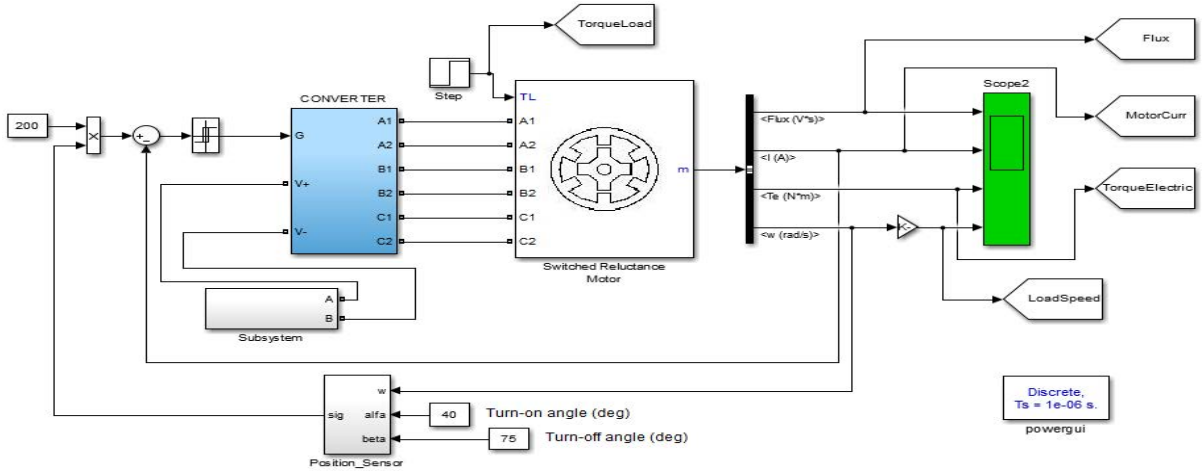

(a) Overall system simulation

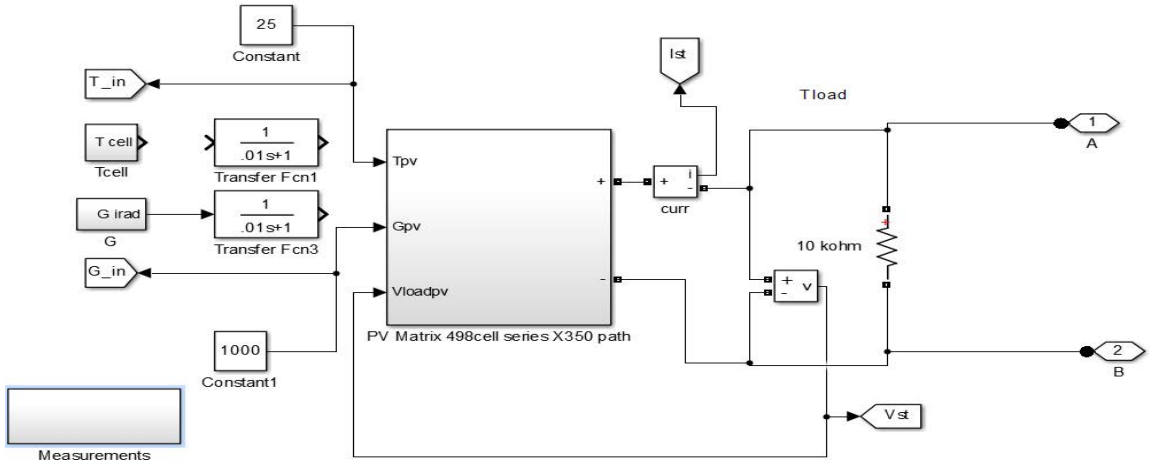

(b) PWP201cells modelling

FIGURE 8. MATLAB/SIMULINK for overall TDM of PWP201/36 unit connected to SRM.

simulated by TDM can supply more current than SDM and DDM with 0.335% error referred to real value and SDM has the lowest source capability with 0.347% error. The DDM has the highest output power capability with 01749% error with respect to real model. Another comparison between RMSE value using TDM, DDM and SDM obtained by different trusted optimizers for PWP201/36 and STM6-40/36 as in Tables 3-4. It can be concluded that RKO could obtain the lowest RMSE value than all optimizers for SDM with minor difference than DDM and TDM as observed in Table 4.

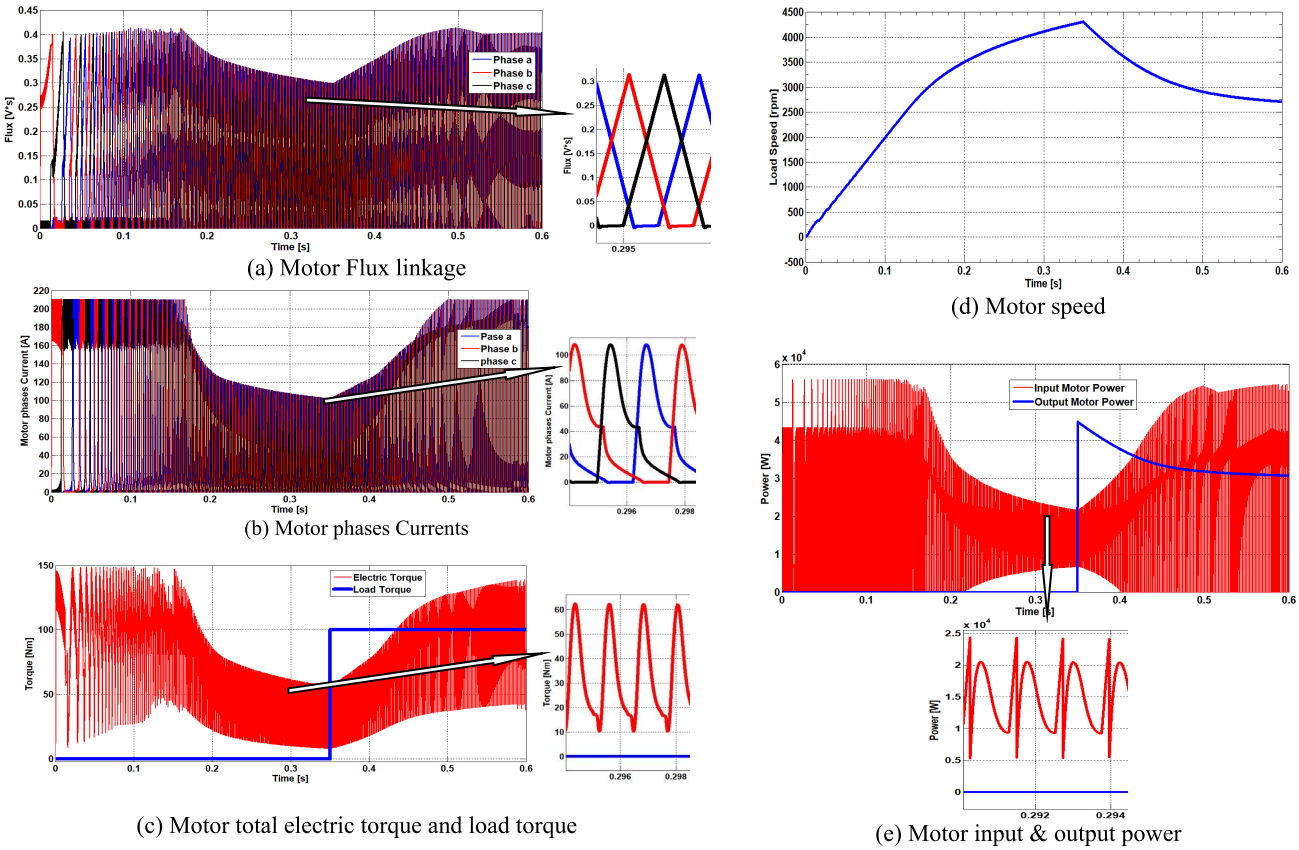

(a) Motor Flux linkage

(b) Motor phases Currents

(c) Motor total electric torque and load torque

(d) Motor speed

(e) Motor input & output power

FIGURE 9. Motor output results and waves.

For STM6-40/36 module, the RKO could reach the lowest RMSE value for TDM as revealed in Table 5.

VI. SIMULATION AND MODEL ASSESSMENT OF TDM OF PWP201/36 MODULE CONNECTED TO SRM

To study and effectively assess the dynamic behavior of the TDM PWP201/36 module, it has been simulated in MATLAB/Simulink and connected to a SRM with nonlinear performance as shown in Fig. 7. The drawn current by the motor depends on the magnetic flux linkage at certain rotor position. For each angle due to the position of the rotor, there will be a different performance characteristic.

A. SYSTEM DESCRIPTION

The complete Simulink simulation model is depicted in Fig. 8(a) which contains mainly of the converter supplied by the output of the PV module ''terminals A and B'' and connected to SRM with its control elements. The detailed PWP201modelling is indicated in Fig. 8(b). The selected motor is 60 kW, three-phase, 6/4 SRM with the detailed data are given in Table 6. The SRM is controlled by a power conditional circuit containing three groups of IGBTs and diodes. The function of IGBTs is to connect the motor stator windings to the source positive terminal where the negative one is connected through the free-wheeling diodes. The required switching on and off angles of the motor currents could be determined by measuring the rotor positions. The motor torque and performance depend mainly on the selected on and off angles which are fed to the drive circuit controller. A suitable current controller is selected to maintain the required currents in controlled ranges.

B. SYSTEM SIMULATION

The PWP201/36 module used in the simulator can be arranged based on the studied load motor voltage and power. A combination of 350 parallel paths with each path contains 498 series cells are required to feed the studied motor by its rated voltage and power. In this case study, the turn on and turn off angles are assumed to be constant at 45 and 75 degrees, respectively. If the drawn current exceeds rated current, the hysteresis current has been reined in using of controller within upper and lower limit as 210 A and 190 A, respectively and the reference current value is 200 A. The motor will rotate as soon as the reference current is applied. The performance of the SRM and PV unit are indicated in Figs.9-10, respectively due to the SRM loading. The operation has two controlled modes: current and voltage. The current mode for the first stage when SRM starts and requires high hysteresis current needed by the high magnetization due to high inertia. After the inertia is reduced to a value requires

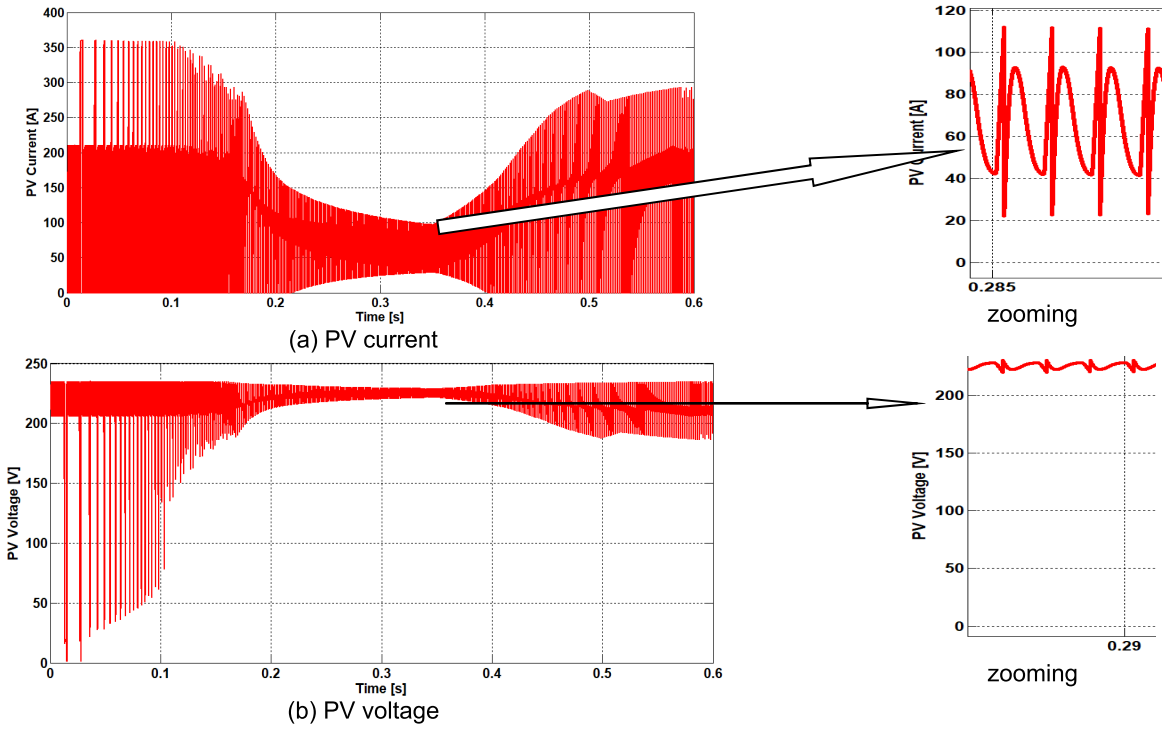

FIGURE 10. PV output current and voltage in time domain.

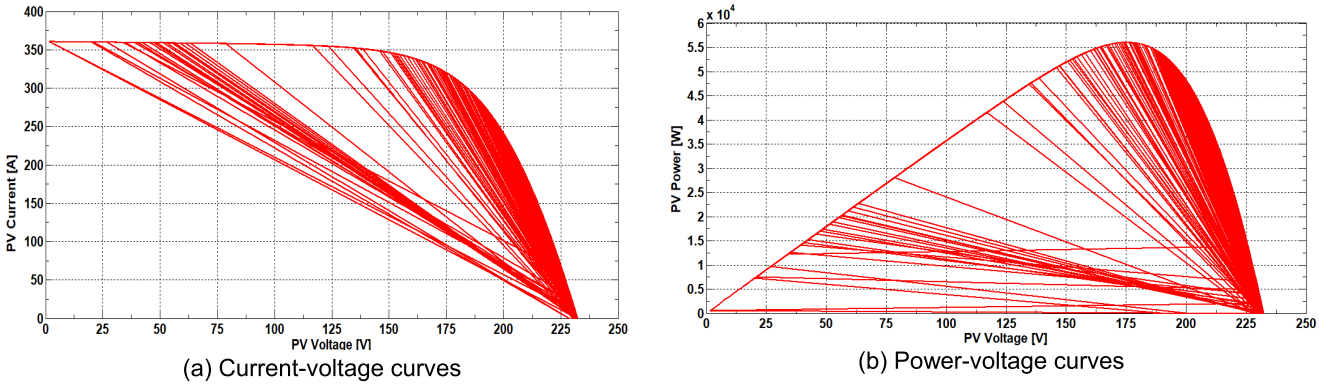

FIGURE 11. I/V and P/V curves of PWP 201.

less current than the selected lower current limit, the mode will be changed to voltage control.

1) CURRENT CONTROLLED MODE

The SRM is started at no load with very high flux to overcome the motor inertia. The current continues to be controlled by converter within the mentioned limits with nearly fixed flux till it starts to decay as the inertia is decreased at nearly about 3100 rpm at 0.18 s as indicated in Fig. 9(a). The same trend can be noticed for no load motor current, electrical torque, and input power but the speed is increased until full no-load speed as shown in Figs. 9 (b)-(e). The behavior of the PWP201/36 module due to the no load condition at this period is indicated in Figs.10(c), and 10(d).

2) VOLTAGE FED MODE

When the motor speed became more than 3100 rpm at 0.18 s and current became less than the reference value, the control strategy will be transferred to voltage fed mode. At this stage, no load motor current, electrical torque, and input power became inversely proportional to the motor speed until stabilizing or loaded.

3) SRM LOADING

Sudden load with 100 Nm torque is connected to the PWP201/36 module through the converter at 0.35 s when the motor speed is 4250 rpm. The controller allows the motor current to be increased again to produce more power and

torque to overcome the required load torque and the motor speed will be reduced rapidly until arrive 2750 rpm.

4) PWP201/36 MODULE SIMULATION BEHAVIOUR

The PV current starts with around 360 A and continues the same up to 0.18 s for the first stage where the SRM starting with no load current which controlled by converter within the preselected limits as shown in Fig. 10(a). During the same period, PV voltage is oscillated around 230 V as shown in Fig.10(b). When the SRM inertia is decreased after 0.18 s and converter is subjected to voltage control mode, the PV current is also decreased till stabilizing and voltage is kept fixed at 230 V without oscillations. Once the SRM is loaded at 0.35 s, the current is going to increase until steadiness at nearly 280 A but voltage has some transients then stay fixed around the 230 V. The corresponding I/V and P/V curves are indicated in Figs.11(a)-(b).

VII. CONCLUSION

A new effort to utilize the RKO optimizer and optimally extract PV parameters using TDM has been addressed. The results have been validated and meaningfully compared with another reliable optimizers which ensures the effectiveness of the RKO. The best RMSE values of the PWP201 and STM6-40/36 TDM modules are 2.050683 mA and 1.712171 mA, respectively. Comprehensive comparisons between SDM, DDM, and TDM results when conducted by the RKO and other well-known optimizers for PWP201/36 and STM6-40/36 modules. RKO scores the lowest RMSE with 2.04 mA for PWP201/36 when SDM is used and 1.7122 mA for STM6-40/36 units when TDM is used. For more confirmation, PWP201/36 module has been represented using MATLAB/SIMULINK environment to evaluate its dynamic performance when connected to SRM. It is worth noting that the RKO proved high capability to deal with the renewable PV systems when connected to SRM as a dynamic load. It is plan to extend this current effort by connected other type of electrical loads to investigate the dynamic responses and principal preformances of the PV units.

Funding: This research was funded by the Deputyship for Research & Innovation, Ministry of Education in Saudi Arabia through the project number "IF_2020_NBU_411".

ACKNOWLEDGMENT

The authors extend their appreciation to the Deputy-ship for Research & Innovation, Ministry of Education in Saudi Arabia for funding this research work through the project number IF_2020_NBU_411.

REFERENCES

[1] D. Wei, M. Wei, H. Cai, X. Zhang, and L. Chen, "Parameters extraction method of PV model based on key points of I-V curve," *Energy Convers. Manage.*, vol. 209, Apr. 2020, Art. no. 112656, doi: 10.1016/j.enconman.2020.112656.

[2] L. M. P. Deotti, J. L. R. Pereira, and I. C. da Silva Júnior, "Parameter extraction of photovoltaic models using an enhanced Lévy flight bat algorithm," *Energy Convers. Manage.*, vol. 221, Oct. 2020, Art. no. 113114, doi: 10.1016/j.enconman.2020.113114.

[3] Y. Tao, J. Bai, R. K. Pachauri, and A. Sharma, "Parameter extraction of photovoltaic modules using a heuristic iterative algorithm," *Energy Convers. Manage.*, vol. 224, Nov. 2020, Art. no. 113386, doi: 10.1016/j.enconman.2020.113386.

[4] G. Xiong, J. Zhang, D. Shi, L. Zhu, and X. Yuan, "Parameter extraction of solar photovoltaic models with an either-or teaching learning based algorithm," *Energy Convers. Manage.*, vol. 224, Nov. 2020, Art. no. 113395, doi: 10.1016/j.enconman.2020.113395.

[5] M. Abdel-Basset, D. El-Shahat, R. K. Chakrabortty, and M. Ryan, "Parameter estimation of photovoltaic models using an improved marine predators algorithm," *Energy Convers Manage*, vol. 227, Jan. 2021, Art. no. 113491, doi: 10.1016/j.enconman.2020.113491.

[6] E. A. Gouda, M. F. Kotb, S. S. M. Ghoneim, M. M. Al-Harthi, and A. A. El-Fergany, "Performance assessment of solar generating units based on coot bird Metaheuristic optimizer," *IEEE Access*, vol. 9, pp. 111616–111632, 2021, doi: 10.1109/ACCESS.2021.3103146.

[7] R. Tamrakar and A. Gupta, "A Review: Extraction of solar cell modelling parameters," *Int. J. Innov. Res. Elect., Electron., Instrum. Control Eng.*, vol. 3, no. 1, pp. 55–60, 2015, doi: 10.17148/IJIREEICE.2015.3111.

[8] K. M. Sallam, M. A. Hossain, R. K. Chakrabortty, and M. J. Ryan, "An improved gaining-sharing knowledge algorithm for parameter extraction of photovoltaic models," *Energy Convers. Manage.*, vol. 237, Jun. 2021, Art. no. 114030, doi: 10.1016/j.enconman.2021.114030.

[9] D. Yousri, H. Rezk, and A. Fathy, "Identifying the parameters of different configurations of photovoltaic models based on recent artificial ecosystem-based optimization approach," *Int. J. Energy Res.*, vol. 44, no. 14, pp. 11302–11322, 2020, doi: 10.1002/er.5747.

[10] M. A. El-Hameed, M. M. Elkholy, and A. A. El-Fergany, "Three-diode model for characterization of industrial solar generating units using manta-rays foraging optimizer: Analysis and validations," *Energy Convers. Manage.*, vol. 219, Sep. 2020, Art. no. 113048, doi: 10.1016/j.enconman.2020.113048.

[11] E. I. Batzelis and S. A. Papathanassiou, "A method for the analytical extraction of the single-diode PV model parameters," *IEEE Trans. Sustain. Energy*, vol. 7, no. 2, pp. 504–512, Apr. 2016, doi: 10.1109/TSTE.2015.2503435.

[12] H. Ibrahim and N. Anani, "Evaluation of analytical methods for parameter extraction of PV modules," *Energy Proc.*, vol. 134, pp. 69–78, Oct. 2017, doi: 10.1016/j.egypro.2017.09.601.

[13] J. Liang, S. Ge, B. Qu, K. Yu, F. Liu, H. Yang, and P. Wei, "Classified perturbation mutation based particle swarm optimization algorithm for parameters extraction of photovoltaic models," *Energy Convers. Manage.*, vol. 203, Jan. 2020, Art. no. 112138, doi: 10.1016/j.enconman.2019.112138.

[14] S. Li, Q. Gu, W. Gong, and B. Ning, "An enhanced adaptive differential evolution algorithm for parameter extraction of photovoltaic models," *Energy Convers. Manage.*, vol. 205, Feb. 2020, Art. no. 112443, doi: 10.1016/j.enconman.2019.112443.

[15] F. J. Toledo and J. M. Blanes, "Analytical and quasi-explicit four arbitrary point method for extraction of solar cell single-diode model parameters," *Renew. Energy*, vol. 92, pp. 346–356, Jul. 2016, doi: 10.1016/j.renene.2016.02.012.

[16] M. H. Qais, H. M. Hasanien, and S. Alghuwainem, "Identification of electrical parameters for three-diode photovoltaic model using analytical and sunflower optimization algorithm," *Appl. Energy*, vol. 250, pp. 109–117, 2019, doi: 10.1016/j.apenergy.2019.05.013.

[17] N. Aoun and N. Bailek, "Evaluation of mathematical methods to characterize the electrical parameters of photovoltaic modules," *Energy Convers. Manage.*, vol. 193, pp. 25–38, Aug. 2019, doi: 10.1016/j.enconman.2019.04.057.

[18] N. Thanh Tong, K. Kamolpattana, and W. Pora, "A deterministic method for searching the maximum power point of a PV panel," in *Proc. 12th Int. Conf. Electr. Eng./Electron., Comput., Telecommun. Inf. Technol. (ECTI-CON)*, Jun. 2015, pp. 1–6, doi: 10.1109/ECTICon.2015.7206928.

[19] T. Easwarakhanthan, J. Bottin, I. Bouhouch, and C. Boutrit, "Nonlinear minimization algorithm for determining the solar cell parameters with microcomputers," *Int. J. Sol. Energy*, vol. 4, no. 1, pp. 1–12, Jan. 1986, doi: 10.1080/01425918608909835.

[20] P. Monal, L. Heistrene, and V. Pandya, "Optimal power flow in power networks with TCSC using particle swarm optimization technique," in *Advances in Electric Power and Energy Infrastructure*. Cham, Switzerland: Springer, 2020, pp. 91–101, doi: 10.1007/978-981-15-0206-4_8.

[21] Q.-V. Pham, S. Mirjalili, N. Kumar, M. Alazab, and W.-J. Hwang, "Whale optimization algorithm with applications to resource allocation in wireless networks," *IEEE Trans. Veh. Technol.*, vol. 69, no. 4, pp. 4285–4297, Apr. 2020, doi: 10.1109/TVT.2020.2973294.
[22] G. Dhiman, "MOSHEPO: A hybrid multi-objective approach to solve economic load dispatch and micro grid problems," *Int. J. Speech Technol.*, vol. 50, no. 1, pp. 119–137, Jan. 2020, doi: 10.1007/s10489-019-01522-4.
[23] Z. Zhu and X. Zhou, "An efficient evolutionary grey wolf optimizer for multi-objective flexible job shop scheduling problem with hierarchical job precedence constraints," *Comput. Ind. Eng.*, vol. 140, Feb. 2020, Art. no. 106280, doi: 10.1016/j.cie.2020.106280.
[24] W. Long, T. Wu, J. Jiao, M. Tang, and M. Xu, "Refraction-learning-based whale optimization algorithm for high-dimensional problems and parameter estimation of PV model," *Eng. Appl. Artif. Intell.*, vol. 89, Mar. 2020, Art. no. 103457, doi: 10.1016/j.engappai.2019.103457.
[25] H. M. Ridha, C. Gomes, and H. Hizam, "Estimation of photovoltaic module model's parameters using an improved electromagnetic-like algorithm," *Neural Comput. Appl.*, vol. 32, no. 16, pp. 12627–12642, 2020, doi: 10.1007/s00521-020-04714-z.
[26] K. Yu, B. Qu, C. Yue, S. Ge, X. Chen, and J. Liang, "A performance-guided JAYA algorithm for parameters identification of photovoltaic cell and module," *Appl. Energy*, vol. 237, pp. 57–241, Mar. 2019, doi: 10.1016/j.apenergy.2019.01.008.
[27] R. B. Messaoud, "Extraction of uncertain parameters of single and double diode model of a photovoltaic panel using salp swarm algorithm," *Measurement*, vol. 154, Mar. 2020, Art. no. 107446, doi: 10.1016/j.measurement.2019.107446.
[28] S. Li, W. Gong, X. Yan, C. Hu, D. Bai, L. Wang, and L. Gao, "Parameter extraction of photovoltaic models using an improved teaching-learning-based optimization," *Energy Convers. Manage.*, vol. 186, pp. 293–305, Apr. 2019, doi: 10.1016/j.enconman.2019.02.048.
[29] W. Long, S. Cai, J. Jiao, M. Xu, and T. Wu, "A new hybrid algorithm based on grey wolf optimizer and cuckoo search for parameter extraction of solar photovoltaic models," *Energy Convers. Manage.*, vol. 203, Jan. 2020, Art. no. 112243, doi: 10.1016/j.enconman.2019.112243.
[30] X. Chen and K. Yu, "Hybridizing cuckoo search algorithm with biogeography-based optimization for estimating photovoltaic model parameters," *Sol. Energy*, vol. 180, pp. 192–206, Mar. 2019, doi: 10.1016/j.solener.2019.01.025.
[31] S.-A. Blaifi, S. Moulahoum, B. Taghezouit, and A. Saim, "An enhanced dynamic modeling of PV module using Levenberg-Marquardt algorithm," *Renew. Energy*, vol. 135, pp. 745–760, May 2019, doi: 10.1016/j.renene.2018.12.054.
[32] Y. Zhang, Z. Jin, X. Zhao, and Q. Yang, "Backtracking search algorithm with Lévy flight for estimating parameters of photovoltaic models," *Energy Convers. Manage.*, vol. 208, Mar. 2020, Art. no. 112615, doi: 10.1016/j.enconman.2020.112615.
[33] F. F. Muhammad, A. W. Karim Sangawi, S. Hashim, S. K. Ghoshal, I. K. Abdullah, and S. S. Hameed, "Simple and efficient estimation of photovoltaic cells and modules parameters using approximation and correction technique," *PLoS ONE*, vol. 14, no. 5, May 2019, Art. no. e0216201, doi: 10.1371/journal.pone.0216201.
[34] A. Ayang, R. Wamkeue, M. Ouhrouche, N. Djongyang, N. Essiane Salomé, J. K. Pombe, and G. Ekemb, "Maximum likelihood parameters estimation of single-diode model of photovoltaic generator," *Renew. Energy*, vol. 130, pp. 111–121, Jan. 2019, doi: 10.1016/j.renene.2018.06.039.
[35] A. Fathy and H. Rezk, "Parameter estimation of photovoltaic system using imperialist competitive algorithm," *Renew. Energy*, vol. 111, pp. 307–320, Oct. 2017, doi: 10.1016/j.renene.2017.04.014.
[36] D. Kler, Y. Goswami, K. P. S. Rana, and V. Kumar, "A novel approach to parameter estimation of photovoltaic systems using hybridized optimizer," *Energy Convers. Manage.*, vol. 187, pp. 486–511, May 2019, doi: 10.1016/j.enconman.2019.01.102.
[37] H. Chen, S. Jiao, A. A. Heidari, M. Wang, X. Chen, and X. Zhao, "An opposition-based sine cosine approach with local search for parameter estimation of photovoltaic models," *Energy Convers. Manage.*, vol. 195, pp. 927–942, Sep. 2019, doi: 10.1016/j.enconman.2019.05.057.
[38] F. Harrou, A. Dairi, B. Taghezouit, and Y. Sun, "An unsupervised monitoring procedure for detecting anomalies in photovoltaic systems using a one-class support vector machine," *Sol. Energy*, vol. 179, pp. 48–58, Feb. 2019, doi: 10.1016/j.solener.2018.12.045.
[39] M. H. Qais, H. M. Hasanien, and S. Alghuwainem, "Parameters extraction of three-diode photovoltaic model using computation and Harris hawks optimization," *Energy*, vol. 195, Mar. 2020, Art. no. 117040, doi: 10.1016/j.energy.2020.117040.
[40] S. I. Selem, A. A. El-Fergany, and H. M. Hasanien, "Artificial electric field algorithm to extract nine parameters of triple-diode photovoltaic model," *Int. J. Energy Res.*, vol. 45, no. 1, pp. 590–604, 2021, doi: 10.1002/er.5756.
[41] M. A. El-Hameed, M. M. Elkholy, and A. A. El-Fergany, "Three-diode model for characterization of industrial solar generating units using Manta-rays foraging optimizer: Analysis and validations," *Energy Convers. Manage.*, vol. 219, Sep. 2020, Art. no. 113048, doi: 10.1016/j.enconman.2020.113048.
[42] I. Ahmadianfar, A. A. Heidari, A. H. Gandomi, X. Chu, and H. Chen, "RUN beyond the metaphor: An efficient optimization algorithm based on Runge Kutta method," *Expert Syst. Appl.*, vol. 181, Nov. 2021, Art. no. 115079, doi: 10.1016/j.eswa.2021.115079.
[43] Y. Du, Y. Liu, and J. A. Ekaterinaris, "Optimized diagonally implicit Runge–Kutta schemes for time-dependent wave propagation problems," *Aerosp. Sci. Technol.*, vol. 93, Oct. 2019, Art. no. 105343, doi: 10.1016/j.ast.2019.105343.
[44] X. Gao, Y. Cui, J. Hu, G. Xu, Z. Wang, J. Qu, and H. Wang, "Parameter extraction of solar cell models using improved shuffled complex evolution algorithm," *Energy Convers. Manage.*, vol. 157, pp. 460–479, Feb. 2018, doi: 10.1016/j.enconman.2017.12.033.
[45] D. T. Cotfas, A. M. Deaconu, and P. A. Cotfas, "Application of successive discretization algorithm for determining photovoltaic cells parameters," *Energy Convers. Manage.*, vol. 196, pp. 545–556, Sep. 2019, doi: 10.1016/j.enconman.2019.06.037.
[46] T. Easwarakhanthan, J. Bottin, I. Bouhouch, and C. Boutrit, "Nonlinear minimization algorithm for determining the solar cell parameters with microcomputers," *Int. J. Sol. Energy*, vol. 4, no. 1, pp. 1–12, Jan. 1986, doi: 10.1080/01425918608909835.
[47] N. T. Tong and W. Pora, "A parameter extraction technique exploiting intrinsic properties of solar cells," *Appl. Energy*, vol. 176, pp. 104–115, Aug. 2016, doi: 10.1016/j.apenergy.2016.05.064.
[48] S. Li, W. Gong, L. Wang, X. Yan, and C. Hu, "A hybrid adaptive teaching–learning-based optimization and differential evolution for parameter identification of photovoltaic models," *Energy Convers. Manage.*, vol. 225, Dec. 2020, Art. no. 113474, doi: 10.1016/j.enconman.2020.113474.
[49] R. M. Rizk-Allah and A. A. El-Fergany, "Emended heap-based optimizer for characterizing performance of industrial solar generating units using triple-diode model," *Energy*, vol. 237, Dec. 2021, Art. no. 121561, doi: 10.1016/j.energy.2021.121561.
[50] H. Rezk and M. A. Abdelkareem, "Optimal parameter identification of triple diode model for solar photovoltaic panel and cells," *Energy Rep.*, vol. 8, pp. 1179–1188, Apr. 2022, doi: 10.1016/j.egyr.2021.11.179.
[51] H. G. G. Nunes, J. A. N. Pombo, S. J. P. S. Mariano, M. R. A. Calado, and J. A. M. Felippe de Souza, "A new high performance method for determining the parameters of PV cells and modules based on guaranteed convergence particle swarm optimization," *Appl. Energy*, vol. 211, pp. 774–791, Feb. 2018, doi: 10.1016/j.apenergy.2017.11.078.
[52] A. R. Jordehi, "Time varying acceleration coefficients particle swarm optimisation (TVACPSO): A new optimisation algorithm for estimating parameters of PV cells and modules," *Energy Convers. Manage.*, vol. 129, pp. 262–274, Dec. 2016, doi: 10.1016/j.enconman.2016.09.085.
[53] X. Gao, Y. Cui, J. Hu, G. Xu, Z. Wang, J. Qu, and H. Wang, "Parameter extraction of solar cell models using improved shuffled complex evolution algorithm," *Energy Convers. Manage.*, vol. 157, pp. 460–479, Feb. 2018, doi: 10.1016/j.enconman.2017.12.033.
[54] G. Xiong, J. Zhang, D. Shi, and Y. He, "Parameter extraction of solar photovoltaic models using an improved whale optimization algorithm," *Energy Convers. Manage.*, vol. 174, pp. 388–405, Oct. 2018, doi: 10.1016/j.enconman.2018.08.053.
[55] H. Zhang, A. A. Heidari, M. Wang, L. Zhang, H. Chen, and C. Li, "Orthogonal nelder-mead moth flame method for parameters identification of photovoltaic modules," *Energy Convers. Manage.*, vol. 211, May 2020, Art. no. 112764, doi: 10.1016/j.enconman.2020.112764.
[56] Z. Chen, L. Wu, P. Lin, Y. Wu, and S. Cheng, "Parameters identification of photovoltaic models using hybrid adaptive Nelder-Mead simplex algorithm based on eagle strategy," *Appl. Energy*, vol. 182, pp. 47–57, Nov. 2016, doi: 10.1016/j.apenergy.2016.08.083.
[57] F. J. Toledo, J. M. Blanes, and V. Galiano, "Two-step linear least-squares method for photovoltaic single-diode model parameters extraction," *IEEE Trans. Ind. Electron.*, vol. 65, no. 8, pp. 6301–6308, Aug. 2018, doi: 10.1109/TIE.2018.2793216.
[58] A. Laudani, F. R. Fulginei, and A. Salvini, "High performing extraction procedure for the one-diode model of a photovoltaic panel from experimental I–V curves by using reduced forms," *Sol. Energy*, vol. 103, pp. 316–326, May 2014, doi: 10.1016/j.solener.2014.02.014.

[59] A. M. Agwa, A. A. El-Fergany, and H. A. Maksoud, "Electrical characterization of photovoltaic modules using farmland fertility optimizer," *Energy Convers. Manage.*, vol. 217, Aug. 2020, Art. no. 112990, doi: 10.1016/j.enconman.2020.112990.
[60] J. Ma, K. L. Man, S.-U. Guan, T. O. Ting, and P. W. H. Wong, "Parameter estimation of photovoltaic model via parallel particle swarm optimization algorithm," *Int. J. Energy Res.*, vol. 40, no. 3, pp. 343–352, Oct. 2016, doi: 10.1002/er.3359.
[61] W. Gong and Z. Cai, "Parameter extraction of solar cell models using repaired adaptive differential evolution," *Sol. Energy*, vol. 94, pp. 209–220, Aug. 2013, doi: 10.1016/j.solener.2013.05.007.
[62] T. Kang, J. Yao, M. Jin, S. Yang, and T. Duong, "A novel improved cuckoo search algorithm for parameter estimation of photovoltaic (PV) models," *Energies*, vol. 11, no. 5, p. 1060, Apr. 2018, doi: 10.3390/en11051060.
[63] D. Oliva, A. A. Ewees, M. A. E. Aziz, A. E. Hassanien, and M. Peréz-Cisneros, "A chaotic improved artificial bee colony for parameter estimation of photovoltaic cells," *Energies*, vol. 10, no. 7, p. 865, 2017, doi: 10.3390/en10070865.
[64] D. Oliva, M. Abd El Aziz, and A. Ella Hassanien, "Parameter estimation of photovoltaic cells using an improved chaotic whale optimization algorithm," *Appl. Energy*, vol. 200, pp. 141–154, Aug. 2017, doi: 10.1016/j.apenergy.2017.05.029.
[65] A. R. Jordehi, "Enhanced leader particle swarm optimisation (ELPSO): An efficient algorithm for parameter estimation of photovoltaic (PV) cells and modules," *Sol. Energy*, vol. 159, pp. 78–87, Jan. 2018, doi: 10.1016/j.solener.2017.10.063.
[66] G. Xiong, J. Zhang, D. Shi, and X. Yuan, "Application of supply-demand-based optimization for parameter extraction of solar photovoltaic models," *Complexity*, vol. 2019, Nov. 2019, Art. no. 3923691, doi: 10.1155/2019/3923691.
[67] A. Shaheen, R. El-Sehiemy, A. El-Fergany, and A. Ginidi, "Artificial hummingbird technique for estimating the electrical parameters of triple-diode models of solar photovoltaic units," *Energy*, to be published.

MOHAMED F. KOTB (Senior Member, IEEE) was born in Monufia, Egypt, in 1960. He graduated from Mansoura University, Egypt. He received the M.Sc. and Ph.D. degrees from Mansoura University, in 1989 and 1998, respectively. He is currently a member of the Electrical Department, Faculty of Engineering, Mansoura University. He has wide experience with industry applications, consultations, and international training. His research interests include electrical power system analyses, renewable energy, smart grids, and application researches.

ATTIA A. EL-FERGANY (Senior Member, IEEE) received the B.Sc., M.Sc., and Ph.D. degrees in electrical power engineering from Zagazig University, Zagazig, Egypt, in 1994, 1998, and 2001, respectively. He has been engaged with the University of Zagazig, since 1998, where he is currently a Full Professor. He has authored/coauthored numerous articles published in the refereed renowned journals. He has been given many awards for distinct international publishing and he has been listed among the top 2% top impactful researchers by Stanford rankings, in 2019, 2020, and 2021. He has again been classified as one of top 1% reviewers in engineering by Publons, in 2018 and 2019. In addition, he has delivered numerous short courses and participated in many field electrical technical studies. His research interest includes the use of intelligent techniques to solve electric power system problems. He is a member of IET. He is an Associate Editor of *AEJ* and *BEEI* journals.

EID ABDELBAKI GOUDA was born in Damietta, Egypt, in 1975. He received the B.Sc. and M.Sc. degrees in electrical engineering from Mansoura University, in 1997 and 2004, respectively, and the Ph.D. degree from the Groupe de Recherche en Électrotechnique et Électronique de Nancy, University Henri Poincare of Nancy, France, in 2011. He is currently a Professor at the Electrical Department, Faculty of Engineering, Mansoura University. His research interests include magnetic gear, electric machine design/control and protection systems, renewable energy, power system analysis, and AI applications in power systems.

AHMED M. AGWA was born in Egypt, in 1979. He received the B.Sc. (Hons.), M.Sc., and Ph.D. degrees in electrical engineering from the Faculty of Engineering, Al-Azhar University, Cairo, Egypt, in 2003, 2009, and 2012, respectively. He is currently an Assistant Professor with Northern Border University, Saudi Arabia (on leave from Al-Azhar University, Egypt, since 2018). He has published many articles in specialized and reputable journals. His research interests include power system analysis, renewable energy systems, and artificial intelligence applications in electrical power engineering.